Carbohydrate Polymers 298 (2022) 120117

Contents lists available at ScienceDirect

Carbohydrate Polymers

journal homepage: www.elsevier.com/locate/carbpol

Microstructural architecture and mechanical properties of empowered cellulose-based aerogel composites via TEMPO-free oxidation

Hassan Ahmad [a,b], Lorna Anguilano [a], Mizi Fan [a,b,*]

[a] Nanocellulose and Biocomposites Research Centre, College of Engineering, Design and Physical Sciences, Brunel University London, UB8 3PH, United Kingdom
[b] Nanoshift ltd, Tintagel House, 92 Albert Embankment, London SE1 7TY, United Kingdom

ARTICLE INFO

Keywords:
Nanocellulose-based aerogel
TEMPO-free oxidation
Microstructure composite mechanism
Crystal structure

ABSTRACT

This paper describes the development of cellulose-based aerogel composites enhanced via a new refinement process. The behaviour and microstructure of treated cellulose aerogel composites are examined including, how the constituents interact and contribute to the overall aerogel composite mechanism. The various forms of cellulose such as treated microcrystalline cellulose (MCT), nanofibrillated cellulose (NFC) and nanocrystalline cellulose (NCC) are also compared. Treated cellulose/Polyvinyl alcohol (PVA) aerogel composites show reinforced microstructural systems that enhance the mechanical property of the aerogels. The specific modulus of treated cellulose aerogels could be increased five-fold compared to the stiffness of untreated cellulose aerogels, reaching specific moduli of 21 kNm/kg. The specific strength of treated cellulose aerogels was also increased by four folds at 1.7 kNm/kg. These results provide insight into the understanding of the morphology and structure of treated cellulose-based aerogel composites.

1. Introduction

Aerogels are an interesting class of nanomaterials possessing very desirable properties including high porosity, low density and low thermal conductivity (Aegerter, Leventis, & Koebel, 2012). They are typically produced using a supercritical extraction technique to replace the liquid component of a gel with a gas (Fricke & Tillotson, 1997) and hold promise for applications in many industries including absorbents, gas sensors, energy storage and supercapacitors (Zhai, Zheng, Cai, Xia, & Gong, 2016; Zhang, Zhai, & Turng, 2017). Their application has thus far been limited however due to the high costs of the raw materials required (Cuce, Cuce, Wood, & Riffat, 2014) and the high energy consumption needed for the supercritical production process. Inorganic aerogels have also been the primary focus of research into aerogels in the past with these being very brittle in nature and thus being limited to applications requiring high strength and toughness (Corma, 1997; Davis, 2002; Dubinin, 1960). This has encouraged research into the development of different composite aerogels that offer superior properties and overcome the current limitations (Ann et al., 2012; Guo et al., 2011; Mohite et al., 2013; Tan, Fung, Newman, & Vu, 2001).

The use of cellulose within aerogels as part of a composite has been widely studied (Aulin, Netrval, Wågberg, & Lindström, 2010; Carlsson et al., 2012; Chen, Yu, Li, Liu, & Li, 2011; Chen, Li, et al., 2021; Chen, Zhang, et al., 2021; Das, Lindström, Sharma, Chi, & Hsiao, 2021; Demilecamps, Beauger, Hildenbrand, Rigacci, & Budtova, 2015; Heise et al., 2021; Liu, Yan, Tao, Yu, & Liu, 2012; Miao, Lin, & Bian, 2020; Pääkkö et al., 2008; Perumal, Nambiar, Moses, & Anandharamakrishnan, 2022; Sehaqui, Zhou, & Berglund, 2011; Zhang, Zhang, Lu, & Deng, 2012; Zou et al., 2021) with results revealing that such aerogels that incorporate cellulose fibrils possess higher elasticity and surface area (Heise et al., 2021; Pääkkö et al., 2008). This is a result of the high aspect ratio of cellulose fibres and the strong hydrogen bonds present which create networks that enhance stress transfer (Pääkkö et al., 2008; Trache et al., 2020). Cellulose, being an abundant, inexpensive and sustainable natural polymer, presents an attractive material choice for researchers attempting to create biocompatible and environmentally friendly products (Dhali, Ghasemlou, Daver, Cass, & Adhikari, 2021; Fang, Hou, Chen, & Hu, 2019; Perumal et al., 2022; Reshmy et al., 2022, 2020). Most aerogels that incorporate cellulose often use the natural fibre as a reinforcement material in nanofibrillar form (Chhajed, Yadav, Agrawal, & Maji, 2019). Aerogels composed of larger cellulose fibres as the sole material have also been developed

* Corresponding author at: Nanocellulose and Biocomposites Research Centre, College of Engineering, Design and Physical Sciences, Brunel University London, UB8 3PH, United Kingdom.
E-mail address: mizi.fan@brunel.ac.uk (M. Fan).

https://doi.org/10.1016/j.carbpol.2022.120117
Received 12 June 2022; Received in revised form 10 September 2022; Accepted 12 September 2022
Available online 16 September 2022

using different synthesis processes including that developed by Feng et al. using Kymene as a cross-linking agent and recycled cellulose from paper waste (Feng, Nguyen, Fan, & Duong, 2015). The aerogel coated with methyltrimethoxysilane (MTMS) exhibited high porosity, high oil absorption capacity, super-hydrophobicity, and very high flexibility (Feng et al., 2015).

A recently developed patented technique for defibrillating raw cellulosic material using sonication and 2,2,6,6-Tetramethylpiperidine-1-oxyl (TEMPO) free oxidation (Fan, 2016) was used to create an aerogel before testing its properties. Acid hydrolysis and mechanical defibrillation are the two primary means of creating nanoscale fibrillated cellulose with the hydrolysis process requiring overly high concentrations of acid and producing relatively low yields (Bondeson, Mathew, & Oksman, 2006; Salimi, Sotudeh-Gharebagh, Zarghami, Chan, & Yuen, 2019). Mechanical defibrillation, however, can damage the microfibril structure by reducing the degree of crystallinity as well as molar mass and may consume a lot of energy depending on the number of passes through a mechanical homogeniser required (Stenstad, Andresen, Tanem, & Stenius, 2008). Different pre-treatments have been used as a method to overcome these limitations presented by mechanical defibrillation with the main agent used during pretreatment being TEMPO-NaBr-NaClO (Isogai, 2021; Pereira, Feitosa, Morais, & Rosa, 2020). However, TEMPO pretreatment is costly, requires the removal of non-cellulose composition and treatment of liquid waste. The TEMPO-free method has been reported to involve lower costs and waste liquid while improving the mechanical performance of the isolated fibres. It involves an oxidation and sonication treatment to defibrillate the raw fibres before using a centrifuge to isolate the fibrils from the suspension (Fan, 2016). Moreover, there are different forms of cellulose depending on the hierarchical scale including micro- and nano-cellulose as well as different types of structures to consider including crystalline and fibrillated. In the present study, PVA/Cellulose aerogels were synthesised using different hierarchical scales of cellulose namely untreated microcrystalline cellulose (MCU), treated microcrystalline cellulose (MCT), nanocrystalline cellulose (NCC) and nanocellulose (NC) which includes nanofibrillated cellulose (NFC) and NCC. The difference is described in the experimental work. Treated micro-cellulose (MCT) is a combination of microcrystalline and branched nanofibrillated cellulose obtained by a partial conversation of the untreated micro-cellulose (MCU). The morphology of the MCU and MCT as well as the mechanical properties of the four types of aerogels were investigated. This study demonstrates that the NC aerogel was found to possess superior mechanical performance.

2. Experimental work

Untreated microcrystalline cellulose termed MCU was converted into four different products including (1) MCT – (thin microcrystalline cellulose with branched nano-fibrillated cellulose (NFC)) obtained by partial conversion of the MCU; (2) NFC – nanocellulose fibrils that are detached from MCTs and may be linked to other NFCs with branched nanocrystalline cellulose (NCC); (3) NCC – nanocellulose crystals that are detached from NFCs and may be linked to other NCCs; (4) NC – nanocellulose that includes NFCs and NCCs before separation methods through decanting the supernatant of the centrifuged nanocellulose. A schematic of the TEMPO-free reaction mechanism is depicted in Fig. 1a and the resulting SEM images of the two nanocellulose derivative profiles, NFC and NCC, is shown in Fig. 1b and c, respectively. The width of the nanocellulose fibrils range between 3 and 20 nm as apparent in Fig. 1bi and bii. Fig. 1d shows the size distribution by intensity of nanocellulose using a 'dynamic light scattering particle size and zeta potential analyser' with a sample size of 2 μl (precision of ±1 %). This was conducted periodically for quality checks with the peak averages presented in Table 1 and an overall *Z*-average of 346.5 d·nm. Cellulose types were incorporated with PVA to compare the following aerogel compositions at 50–50 %: MCU-PVA, MCT-PVA, NCC-PVA and NC-PVA. Pure MCU, MCT and PVA were also prepared to compare against.

Table 1
Quantitative measurements of the peak sizes in Fig. 1d.

	Size (d·nm)	% intensity	St Dev (d·nm)
Peak 1	361.6	94.9	164.5
Peak 2	5082	5.1	561.3
Peak 3	~90	n/a	n/a

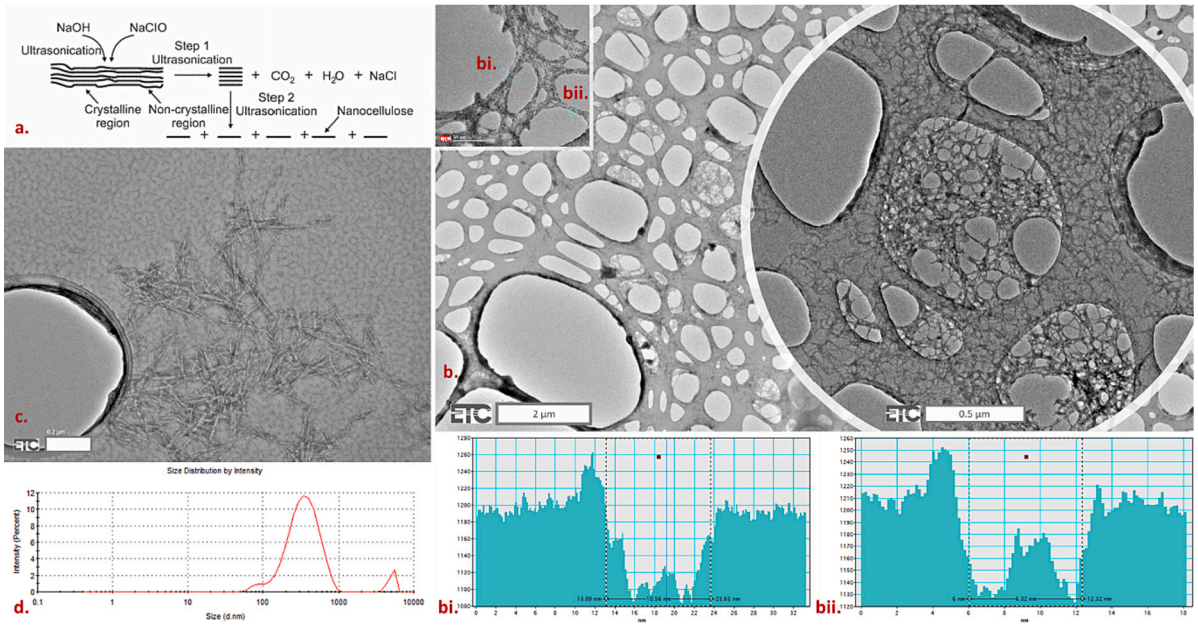

Fig. 1. (a) Schematic of the TEMPO-free NC fabrication process; (b) TEM micrographs of the NFC network with the graphs in bi and bii corresponding to the width of the fibrils; (c) TEM micrograph of NCC; (d) size distribution of NC analysed by intensity.

2.1. Materials

For analytical and consistency purposes, untreated microcrystalline cotton cellulose (MCU), 20 μm was purchased from Sigma Aldrich. 98+ % hydrolysed Polyvinyl alcohol (PVA), Mw = 146–186,000 was purchased from Sigma Aldrich. Purified deionised water, 0 μS was used throughout this study via a Biopure 600-unit (Veolia Water Technologies). Sodium hypochlorite (NaClO), 12.5 % and sodium hydroxide (NaOH), analytical grade 98 % were obtained from Sigma Aldrich and Fisher Scientific, respectively.

2.2. Treated micro-cellulose (MCT) preparation

MCU was suspended in de-ionised water. The suspension was swelled and later oxidised using NaOH and NaClO, respectively. The oxidation reaction was high-shear mixed using a Polytron system PT 2500 E (Kinematica ag) and an IKA HB 10 heating bath to keep the mixture mixed at 45 °C, for 30 min. The homogenised slurry was then washed to pH 7 through cycles of centrifugation, using de-ionised water, followed by dialysis cycles for 48 h to remove any salts and achieve an electrical conductance of <100 μS. An approximate yield of 40 % nanocellulose crystals (NCC) is produced through this process and was consequently separated through centrifugation for this study. Due to the difficulty of separating NFC from the MCT, the remaining 60 % nanocellulose fibrils were termed treated micro-cellulose (MCT) in this paper and were used for this investigation with consequent aerogel preparation. A sample of nanocellulose (NC) was also investigated in this study.

2.3. Aerogel sample preparation

5 wt% stock suspensions of MCU, MCT, NCC, NC and PVA were prepared. Desired amounts of each cellulose type were suspended in deionised water by high-shear mixing at 10,000 rpm for 10 min at 22 °C (ambient temperature) to maximise the cellulose dispersion (Fig. 2) due to the deagglomeration caused by the electrostatic forces within the vortex; while PVA was dissolved in deionised water in a round-bottom flask and stirred at low shear for 2 h in a heating bath at 85 °C. The combined mixtures were diluted to compose final suspensions of MCU-PVA, MCT-PVA, NCC-PVA and NC-PVA at 2.5:2.5 wt% for each composition. The suspensions were homogenised using the shear mixer for 10 min at 10,000 rpm under room temperature. The suspension was later poured on 100 × 100 × 10 mm aluminium foil moulds and frozen in a liquid nitrogen bath. The frozen samples were freeze-dried (ice sublimed) at −51 °C for 120 h via a lyophiliser (Alpha 1–2 LD chamber) to attain the aerogel composites.

2.4. Characterisations

2.4.1. Transmission electron microscopy (TEM)

The suspension structure of cellulose fibres with PVA (MCU-PVA and MCT-PVA) were examined using a JEOL TEM-2100F microscope operated at 200 kV. Cellulose suspensions were negative stained using 1 % uranyl acetate before they were drop-cast onto carbon holey film support copper 200 mesh grids. The holey carbon grids had been glow-discharged beforehand for 20 s using an Agar Turbo Carbon Coater set at 10 mA. Excess sample and stain were wicked away with blotting paper. Prior to entry into the microscope, samples were plasma cleaned for 30 s using a Gatan Solarus. Fast Fourier transform (FFT) images were also obtained to measure distances between atomic planes. TEM lattice structures were analysed via the GMS 3 Gatan software.

2.4.2. Scanning electron microscope (SEM)

The developed aerogel microstructures were characterized through scanning electron microscopy using a Zeiss Supra 35VP FEG-SEM. Cross-sections of the aerogel samples were cut via single-edge razor blades. The electron high tension (EHT) was set at 5 kV and imaging was carried out using the SE2 detector. Due to the non-conductive nature, samples were sputter-coated with a thin layer of gold prior to imaging using a Polaron-SC7640 Sputter Coater for 2 min.

2.4.3. Apparent density

An analytical balance precise to ±0.005 mg and a digital Vernier calliper precise ±0.005 mm was used to measure the dry mass and volume of aerogel samples, respectively. Average densities of four samples per composition were calculated (dry mass over volume) (Fig. 5b).

2.4.4. Mercury intrusion porosimetry

A Micromeritics AutoPore V 9620 was used to measure the specific surface area, bulk density and porosity to characterise the NC-PVA aerogel measuring the pore size distribution within a range of 0.003–600 μm.

2.4.5. Compressive strength

Aerogel composite samples were cut to 20 × 20 × 10 mm via a diamond band saw for compression testing. The test was conducted using an INSTRON 5900 with a 50 kN load cell in a controlled environment of 23 °C and relative humidity of 45 % in accordance with BS EN ISO 604. The applied load rate was set to 1 mm/min until a 60 % strain was realised. The load was applied perpendicular to the axial grain orientation of the aerogel samples. Averages of compressive modulus and yield strength of four samples were taken.

2.4.6. X-ray diffraction (XRD)

X-ray diffraction patterns of untreated (MCU, MCU-PVA aerogel) and

Fig. 2. Preparation steps involved in the production of the aerogel composites including, centrifugation of treated cellulose, aerogel suspensions and lyophilisation.

treated (MCT, MCT-PVA aerogel) samples were obtained using the Bragg-Brentano Bruker D8 Advance with Copper tube and LynxEye position sensitive detector. Samples were scanned between 2θ of 5° to 100° with increments of 0.01° at a scan speed of 1.2 s/step using the Cu Kα radiation (λ = 1.540596 Å). The XRD patterns were interpreted using software, Bruker Evaluation Diffrac, Topas and OriginPro.

The Crystallinity Index (CrI) was calculated using the following equation (Segal, Creely, Martin, & Conrad, 1959):

$$CrI = \frac{(I_{002} - I_{am})}{I_{002}} \times 100$$

3. Results and discussion

3.1. Comparison of MCU and MCT suspensions in PVA dispersions

Fig. 3a and b show TEM micrographs of MCT-PVA and MCU-PVA suspensions, respectively. It is clear that there is a significant difference between the two suspensions. MCT-PVA (Fig. 3a) shows a homogenous suspension with a large, almost complete web-like network between the fibres. This is highlighted in the inset image of Fig. 3a. The larger MCT fibres are small in number however are not separated from the network of the finer fibrils. Rather they are within the network structure due to their open surface of branched fibres, which are of similar aspect ratio to the surrounding finer fibrils, and therefore able to form a web-like network structure. In comparison, the suspension of MCU-PVA (Fig. 3b) struggles to form a network structure, displaying large voids and bulkier fibres. Also, there seem to be several large grey sheets, depicting PVA, where more voids would otherwise be formed. This infers that there may also be MCU fibres without much bonding formed with PVA due to dispersion and/or characteristics of MCU fibres. Hence, this could be the reason for PVA preferentially bonding with itself to form the displayed grey sheets even though both suspensions were shear mixed at 10,000 rpm. These PVA sheets are not displayed in MCT-PVA. This may very well be due to the more homogenous network dispersion of MCT as well as the higher aspect ratio of the fibres granting more active –OH surfaces to bond with PVA. This also infers that the PVA is binding along the increased surface of the highly dispersed MCT fibres. Thus, the network of fibres is more strongly linked as displayed by the darker patches at the joints of the fibre network (inset image of Fig. 3a). The darker shade of the MCU fibres explains a thicker dimension with a very low aspect ratio compared to the MCT fibres whereby the shade of grey is marginally darker than the fine fibrils. The overall reduction in fibre dimension sizes, as well as the branched network structure of MCT particles, may aid in the packing arrangement with PVA as the smaller MCT particles may occupy the cavities between the larger particles during freeze-casting, entrapping longer chains of particles – i.e. forming more continuous and branched solid layers once lyophilised. This may relate to a more homogenous aerogel density and hence increased mechanical strength due to enhanced efficiency in load transfer. This distinction in the dispersity of both suspensions sets a significant discrepancy in freeze-casting and thus in the final aerogel morphology.

3.2. Morphology of MCU-PVA and MCT-PVA aerogel composites

The microstructure of the lyophilised cellulose aerogels is an important consideration in distinguishing the mechanical and physical properties of the aerogel composites (De France et al., 2021). The architectural structure of the aerogels determines their effectiveness to dissipate stress when loaded (Liu et al., 2022). It is apparent from Fig. 3c and d that both MCU- and MCT-PVA aerogel composites form a layered architectural lamellar structure though are considerably different. The full cross-section of MCT-PVA aerogel in Fig. 3c shows an ordered lamellar structure with a growing tree-like profile. It can be seen that when comparing the lower (Fig. 3cii) and upper (Fig. 3ci) sections of Fig. 3c the vertical lamellae layers are increasingly separating in the lateral direction, displaying dendritic growth. This is due to the perpendicular growth of the layers. The thickness of the upper section can be linked to the freeze-casting stage, whereby the solidification velocity of the growing ice crystals in the vertical direction decreases which results in increasing lateral growth. On the other hand, MCU-PVA aerogel displays a more incoherent structure, containing ordered and disordered regions. The upper (Fig. 3di) and lower (Fig. 3dii) sections of Fig. 3d portray a similar effect to the MCT-PVA in that the lamellar layers grow thicker in the upper region. However, the lamellar layers in Fig. 3di increase in thickness with wider cavities as opposed to the occurrence of dendritic growth in Fig. 3ci. Nevertheless, the thickness of the MCU-PVA layers is still a fraction of the MCT-PVA layers. As shown in Fig. 3ciii, the MCT-PVA grow notable larger in thickness filling more of the voids in between in contrast to Fig. 3diii where the layers grow up to half the thickness of MCT-PVA with slightly wider cavities. The larger voids are also displayed in the lower (Fig. 3dii) section of MCU-PVA in comparison to MCT-PVA where the lower (Fig. 3cii) section shows an increased number of lamellar layers with a large number of bridges in-between the layers that occupy the majority of the voids. As discussed earlier, this may be due to the packing arrangement of PVA with the branched MCT network in suspension. This is desirable in reducing thermal conductivity, whereby the increased vertical layers increase lateral heat flow cycles of conduction and convection. The bridges act as struts providing a more tortuous heat flow path/system as well as giving way to an increased number of air pockets while reducing the pocket size. In addition to increasing porosity, the struts also increase the sturdiness of the composite. Under stress, these bridges may aid in the energy distribution more efficiently and thus increase the aerogel stiffness. The overall microstructural observation of the two aerogels is linked back to the distribution of their suspensions before freeze-casting. The incoherent structure of MCU-PVA aerogel (Fig. 3d) is similar to its irregular and cluttered suspension (Fig. 3b). Similarly, the layered and dendritic patterns of MCT-PVA aerogel (Fig. 3c) are parallel to the homogenous network structure of its suspension (Fig. 3a). Furthermore, a notable amount of fibres is perceived in the MCU composite. This may be due to the bulkiness of the MCU fibres in suspension, whereby the PVA binds around the low surface area of –OH active sites of MCU fibres. This means for a 50:50 % ratio of MCU-PVA formulation, excess PVA allows for more intra-PVA bonding. This may also mean that the PVA in the MCU aerogel composites contributes more towards the strength of the composite as the MCU fibres do not form a network and that the needle-like patterns may represent PVA layers. Moreover, the characteristics of the formed aerogel were assessed in terms of the specific surface area, bulk density and porosity through mercury intrusion porosimetry. A sample of NC-PVA aerogel was found to possess a specific surface area of 119.63 m^2/g with a median pore diameter of 31.3 nm at 59.82 m^2/g and a bulk density of 0.0613 g/ml with a porosity of 94.5 %. Noticeable compression of the sample was observed following analysis which means that the true porosity is expected to be higher than the recorded result as compression causes pores within the sample to close. In addition, mercury intrusion may destroy the nanofibrillar network of the cellulose aerogel which may have further reduced the porosity result recorded from the possible true value (Pircher et al., 2016). The porosity and specific surface area of the sample confirms it to be an aerogel as detailed in (Aegerter et al., 2012).

3.3. Influence of cellulose treatment on the basal spacing of MCT-PVA aerogel

The MCU-PVA and MCT-PVA composites and individual raw materials (MCU, MCT, PVA) were analysed using XRD to ascertain whether the composite manufacturing process incurs structural (d-spacing) or crystallinity changes (Fig. 4). It can be observed that the cellulose peaks both of MCU and MCT shift once PVA is inserted into the structure. The shifts in the graph indicate the changes in d-spacing caused by the

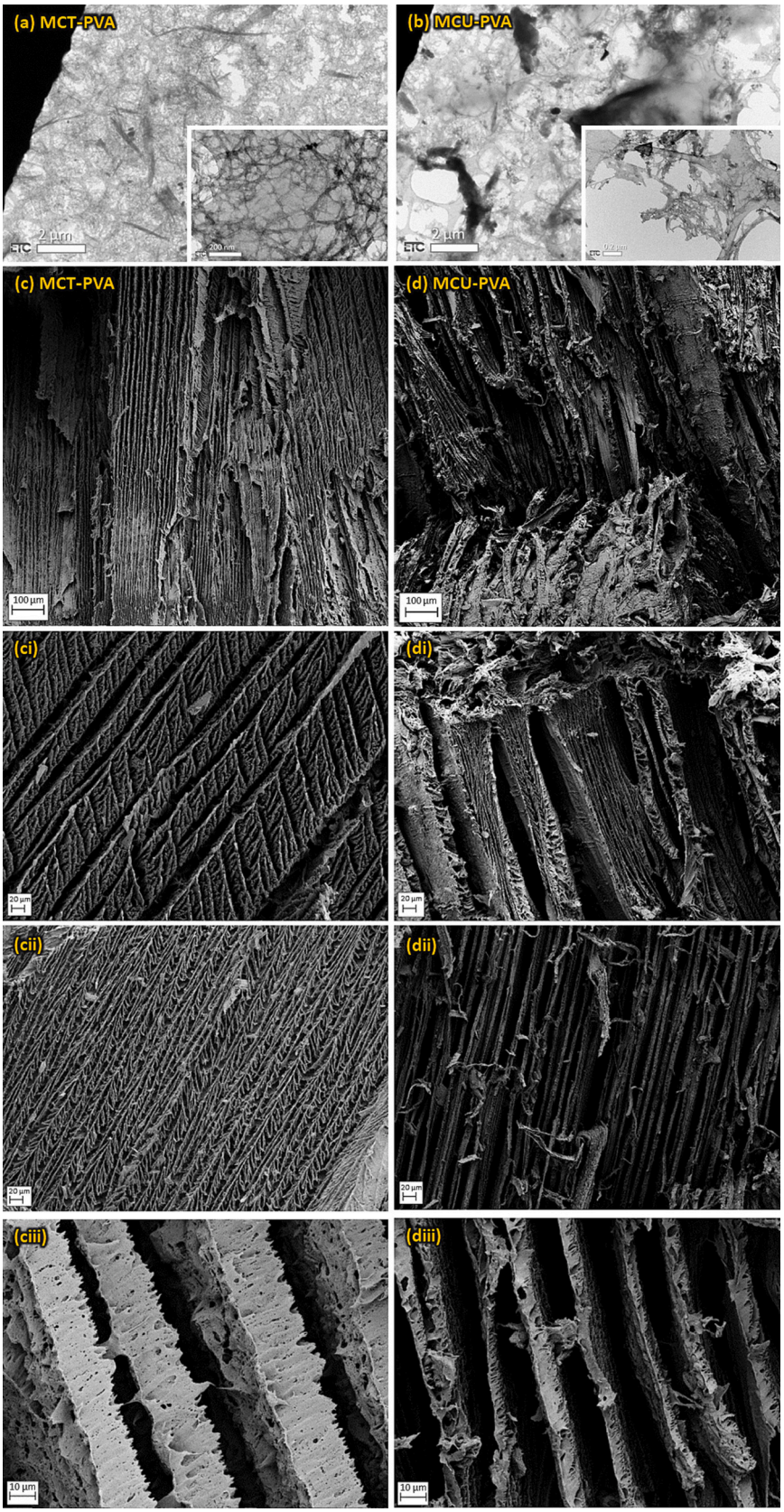

Fig. 3. TEM micrographs of (a) MCT-PVA suspension and (b) MCU-PVA suspension; Comparative visual analysis of MCU-PVA and MCT-PVA SEM cross-sectional images of (c) MCT-PVA aerogel with corresponding separate images of morphological profiles (ci)–(ciii) and (d) MCU-PVA aerogel with corresponding profiles of separate images (di)–(diii).

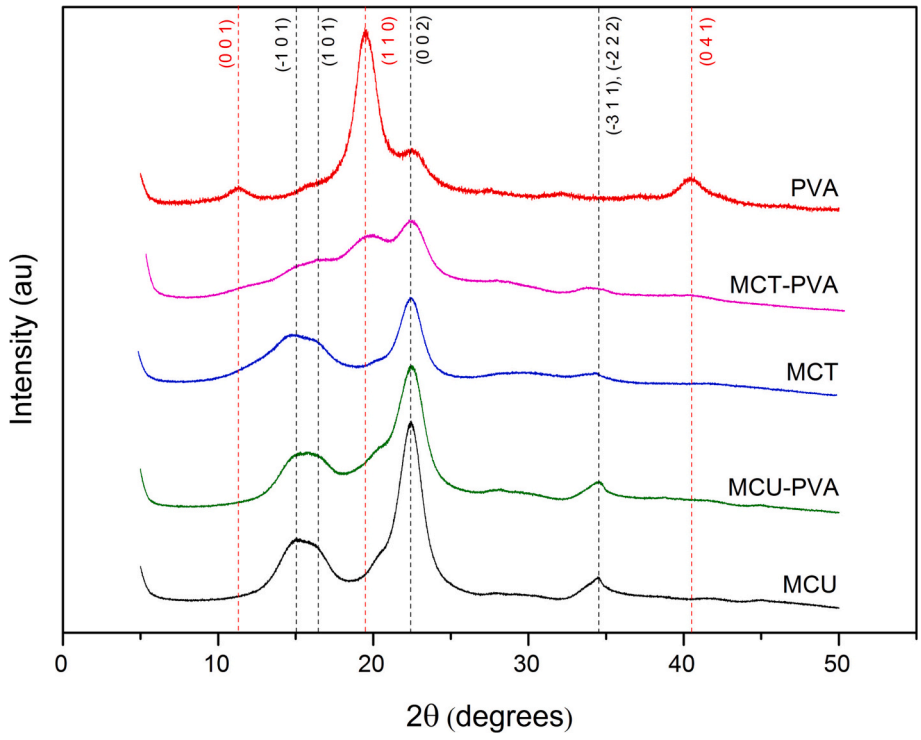

Fig. 4. XRD spectrums of PVA aerogel composites.

presence of PVA in the structure (Table 2). In particular, it can be observed that d-spacing decreases both in MCU and MCT, however, the phenomenon is more pronounced in the MCT (around 3 times larger). The phenomenon is orientation-dependent, strongest along the (0, 0, 2) plane in both materials. Moreover, the MCU samples do not show changes in crystallinity (~80 %) before and after the manufacturing of the composites as the cellulose and PVA crystallise separately. The full width at half maximum (FWHM) for the cellulose [0, 0, 2] plane calculated for each composite and raw material was found to be 1.58 ± 0.03, indicating a crystalline size of ~60 Å. However, small changes can be observed in the MCT. The crystallinity remains 50 % both for MCT and for the MCT-PVA composite, however, the cellulose crystallite size seems to decrease from ~70, with a FWHM of 1.26 for the [0, 0, 2] of the MCT to ~60 Å with a FWHM of 1.6. Consequently, the results seem to indicate that the crystalline structure of the MCT allows for larger compressive stresses to its lattice which induces a relatively wider shift of d-spacing relative to the untreated cellulose.

PVA has a semi-crystalline nature with a monoclinic unit, whereby it has both crystalline and amorphous domains in the matrix (Bunn, 1948; Colvin, 1974). Observing the PVA spectrum against the other composite spectra, it can be seen that the (0, 0, 1) plane of the PVA is not visible in MCU-PVA, which means that the peak in MCT-PVA may not be attributed to the PVA (0, 0, 1) peak, rather more directly to the cellulose II of the MCT peak. The reduction of the (0, 0, 1) peak may be attributed to the random dispersion of cellulose, inferring that possible distortion of the structure has occurred in the (0, 0, 1) direction/plane and hence this would be due to the bonding of PVA with cellulose. A similar reduction is shown for the (0, 4, 1) peak of PVA in MCU- and MCT-PVA, while the (1, 1, 0) peak can only be seen in MCT-PVA.

3.4. Compressive property of cellulose-PVA aerogels

The compressive stiffness of aerogel composites is typically dependent on the effectiveness of the microstructure in its ability to efficiently transfer the applied stress and is also dependent on the solid content which increases the density resulting in a stiffer composite. It can be seen that the composite graphs follow a generic compressive profile where the composites yield between 10 and 20 % strain and plastic deformation occurs until the aerogels start to deform exponentially beyond ~30 % strain (Fig. 5a). MCT-PVA possesses significantly higher strength and stiffness compared to MCU-PVA (Table 3). This is despite MCU-PVA possessing a higher density than MCT-PVA (Fig. 5b). There is a 3.6-fold higher specific modulus and a 2.9-fold higher specific strength in MCT relative to the MCU composite (Table 3). The increased stiffness and strength of MCT-PVA may be a result of the superior microstructure and bonding interface between MCT and PVA. Evidence for this may be

Table 2
d-value of the PVA aerogel composites.

[HKL]	Specimen	MCU-PVA		MCT-PVA		Overall change	
		d-value (Å)	Δ d (Å)	d-value (Å)	Δ d (Å)	d-value change	Δ d MCT/ Δ d MCU
[0,0,2]	Composite	3.93	−0.03	3.95	−0.01	0.03	0.4
	Cellulose	3.95		3.96		0.01	
[−3,1,1], [−2,2,2]	Composite	2.59	−0.01	2.64	−0.05	0.05	−1.9
	Cellulose	2.60		2.69		0.01	
[−1,0,1]	Composite	5.81	−0.07	5.88	−0.19	0.07	2.5
	Cellulose	5.88		6.07		0.18	
[1,0,1]	Composite	5.34	−0.05	5.41	−0.03	0.07	−0.4
	Cellulose	5.39		5.44		0.05	

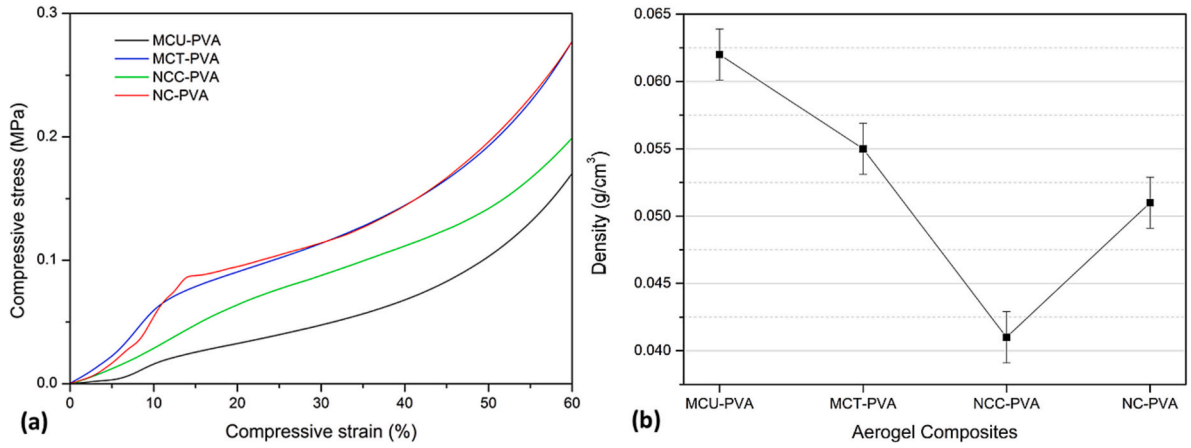

Fig. 5. (a) Stress-strain graphs of the different PVA aerogel composites and (b) comparing their densities.

Table 3
Mean compressive property of the PVA aerogel composites.

	Density (g/cm^3)	Specific modulus (E/ρ) (±0.01 kNm/kg)	Specific strength (σ/ρ) (±0.01 kNm/kg)	Yield strain (%)
MCU-PVA	0.062	4.45	0.42	14.88
MCT-PVA	0.055	15.79	1.24	12.90
NCC-PVA	0.041	9.13	1.29	18.31
NC-PVA	0.051	20.55	1.71	17.13

found in the TEM micrographs (Fig. 3) where the oxidised MCT fibres appear to possess higher aspect ratios and are more branched as per MCU bulk fibre. Firstly, the increased aspect ratio due to the splitting of cellulose fibrils via oxidation adopts additional surfaces of –OH active sites for PVA bonding to occur. This yields an increased number of PVA reinforced cellulose layers and thus stiffens the overall macro sheet layer, which stacks together to form the aerogel composite. Secondly, the chain of connected branched fibres adopts a more effective load distribution which increases the stiffness and strength. The increased stiffness from these phenomena may also contribute to the increased mean yield stress of the MCT aerogel. It is thought that the increased stiffness and strength observed in treated cellulose composites could at least partially be attributed to the increased number of –OH active sites in correspondence to increasing surface area as well as the branched network effect.

NC-PVA was also investigated to understand how a composite MCT and NCC behave. It can be seen from Fig. 5 that the mechanical properties of NC-PVA outperform that of NCC-PVA and MCT-PVA individually. NCC-PVA possessed the lowest density among the four composites and seems to have lowered the density of the overall NC-PVA composite. Combining NCC and MCT seems to have improved the underlying microstructure of the composite possibly through crosslinks between the two agents and PVA. This has resulted in significantly higher stiffness and strength while reducing the density of the overall NC-PVA composite (Table 3).

4. Conclusions

The behaviour and structure of their suspensions and the developed aerogels have been thoroughly investigated to determine their physical and mechanical properties. MCT-PVA suspensions showed expansive robust network structures due to the homogenous network dispersion of MCT as well as the higher aspect ratio of the fibres in comparison to MCU granting more active –OH surfaces to bond with PVA and adding to the packing arrangement with PVA. This has affected the architecture of the developed MCT-PVA aerogel showing ordered lamellar structures with dendritic growth that displayed superior strength and stiffness to the MCU-PVA aerogel composite. XRD and SEM explained the effective load distribution under compressive stress due to the formation of bridges in the microstructure, alteration of crystallinity in basal spacing and high aspect ratio. Furthermore, within the MCT-PVA, it was found that the NC-PVA particularly (which comprises NFC and NCC) possesses the greatest mechanical properties with a specific modulus of 21 kNm/kg and specific strength of 1.7 kNm/kg. Overall, this paper presents new findings in the field of nanocellulose material science including a new refinement process to enhance the properties of cellulose-based aerogel composites while also boosting the commercial value in a wide range of application prospects due to reduced costs associated with the TEMPO reagent and the effluent treatment. The enhanced microstructural system leads to strengthened mechanical properties, which in turn improves the application of aerogel materials in areas where high strength and toughness are required.

CRediT authorship contribution statement

Hassan Ahmad: Conceptualization, Methodology, Software, Validation, Formal analysis, Investigation, Resources, Data curation, Writing – original draft, Writing – review & editing, Visualization, Project administration. **Lorna Anguilano:** Software, Validation, Writing – review & editing. **Mizi Fan:** Writing – review & editing, Supervision, Project administration.

Declaration of competing interest

The authors declare that they have no known competing financial interests or personal relationships that could have appeared to influence the work reported in this paper.

Data availability

The data that has been used is confidential.

References

Aegerter, M. A., Leventis, N., & Koebel, M. M. (2012). *Aerogels handbook*.
Ann, M., Meador, B., Malow, E. J., Silva, R., Wright, S., Quade, D.Cakmak, M., … (2012). Mechanically strong, flexible polyimide aerogels cross-linked with aromatic triamine. *ACS Applied Materials & Interfaces, 4*(2), 536–544.
Aulin, C., Netrval, J., Wågberg, L., & Lindström, T. (2010). Aerogels from nanofibrillated cellulose with tunable oleophobicity. *Soft Matter, 6*(14), 3298–3305.
Bondeson, D., Mathew, A., & Oksman, K. (2006). Optimization of the isolation of nanocrystals from microcrystalline cellulose by acid hydrolysis. *Cellulose, 13*(2), 171–180.

Bunn, C. W. (1948). Crystal structure of polyvinyl alcohol. *Nature, 161*(4102), 929–930.
Carlsson, D. O., Nyström, G., Zhou, Q., Berglund, L. A., Nyholm, L., & Strømme, M. (2012). Electroactive nanofibrillated cellulose aerogel composites with tunable structural and electrochemical properties. *Journal of Materials Chemistry, 22*(36), 19014–19024.
Chen, W., Yu, H., Li, Q., Liu, Y., & Li, J. (2011). Ultralight and highly flexible aerogels with long cellulose I nanofibers. *Soft Matter, 7*(21), 10360–10368.
Chen, Y., Li, S., Li, X., Mei, C., Zheng, J., Shiju, E.Jiang, S., … (2021). Liquid transport and real-time dye purification via lotus petiole-inspired long-range-ordered anisotropic cellulose nanofibril aerogels. *ACS Nano, 15*(12), 20666–20677. https://doi.org/10.1021/ACSNANO.1C10093/SUPPL_FILE/NN1C10093_SI_003.MP4
Chen, Y., Zhang, L., Yang, Y., Pang, B., Xu, W., Duan, G.Xu, W., … (2021). Recent progress on nanocellulose aerogels: Preparation, modification, composite fabrication,applications. *Advanced Materials, 33*(11), 2005569. https://doi.org/10.1002/ADMA.202005569
Chhajed, M., Yadav, C., Agrawal, A. K., & Maji, P. K. (2019). Esterified superhydrophobic nanofibrillated cellulose based aerogel for oil spill treatment. *Carbohydrate Polymers, 226*, Article 115286. https://doi.org/10.1016/J.CARBPOL.2019.115286
Colvin, B. G. (1974). Crystal structure of polyvinyl alcohol. *Nature, 248*(5451), 756–759.
Corma, A. (1997). From microporous to mesoporous molecular sieve materials and their use in catalysis. *Chemical Reviews, 97*, 2373–2419.
Cuce, E., Cuce, P. M., Wood, C. J., & Riffat, S. B. (2014). Toward aerogel based thermal superinsulation in buildings: A comprehensive review. *Renewable and Sustainable Energy Reviews, 34*, 273–299.
Das, R., Lindström, T., Sharma, P. R., Chi, K., & Hsiao, B. S. (2021). Nanocellulose for sustainable water purification. *Chemical Reviews*. https://doi.org/10.1021/ACS.CHEMREV.1C00683/SUPPL_FILE/CR1C00683_SI_001.PDF
Davis, M. E. (2002). Ordered porous materials for emerging applications. *Nature, 417*, 813–821.
De France, K., Zeng, Z., Wu, T., Nyström, G., De France, K., Zeng, Z.Nyström, G., … (2021). Functional materials from nanocellulose: Utilizing structure-property relationships in bottom-up fabrication. *Advanced Materials, 33*(28), Article 2000657. https://doi.org/10.1002/ADMA.202000657
Demilecamps, A., Beauger, C., Hildenbrand, C., Rigacci, A., & Budtova, T. (2015). Cellulose–silica aerogels. *Carbohydrate Polymers, 122*, 293–300. https://doi.org/10.1016/J.CARBPOL.2015.01.022
Dhali, K., Ghasemlou, M., Daver, F., Cass, P., & Adhikari, B. (2021). A review of nanocellulose as a new material towards environmental sustainability. *Science of the Total Environment, 775*. https://doi.org/10.1016/J.SCITOTENV.2021.145871
Dubinin, M. M. (1960). The potential theory of adsorption of gases and vapors for adsorbents with energetically nonuniform surfaces. *Chemical Reviews, 60*(2), 235–241.
M. Fan (2016). Patent No. WO 2016/055782 A1. WIPO.
Fang, Z., Hou, G., Chen, C., & Hu, L. (2019). Nanocellulose-based films and their emerging applications. *Current Opinion in Solid State and Materials Science, 23*(4). https://doi.org/10.1016/J.COSSMS.2019.07.003
Feng, J., Nguyen, S. T., Fan, Z., & Duong, H. M. (2015). Advanced fabrication and oil absorption properties of super-hydrophobic recycled cellulose aerogels. *Chemical Engineering Journal, 270*, 168–175.
Fricke, J., & Tillotson, T. M. (1997). Aerogels: Production, characterization, and applications. *Thin Solid Films, 297*(1–2), 212–223.
Guo, H., Ann, M., Meador, B., Mccorkle, L., Quade, D. J., Guo, J.Sprowl, G., … (2011). Polyimide aerogels cross-linked through amine functionalized polyoligomeric silsesquioxane. *ACS Applied Materials & Interfaces, 3*(2), 546–552.
Heise, K., Kontturi, E., Allahverdiyeva, Y., Tammelin, T., Linder, M. B., Nonappa, & Ikkala, O. (2021). Nanocellulose: Recent fundamental advances and emerging biological and biomimicking applications. *Advanced Materials, 33*(3), Article 2004349. https://doi.org/10.1002/ADMA.202004349
Isogai, A. (2021). Emerging nanocellulose technologies: Recent developments. *Advanced Materials, 33*(28). https://doi.org/10.1002/ADMA.202000630
Liu, H., Xu, T., Cai, C., Liu, K., Liu, W., Zhang, M.Du, H., … (2022). Multifunctional superelastic, superhydrophilic, and ultralight nanocellulose-based composite carbon aerogels for compressive supercapacitor and strain sensor. *Advanced Functional Materials, 32*(26), 2113082. https://doi.org/10.1002/ADFM.202113082
Liu, S., Yan, Q., Tao, D., Yu, T., & Liu, X. (2012). Highly flexible magnetic composite aerogels prepared by using cellulose nanofibril networks as templates. *Carbohydrate Polymers, 89*(2), 551–557.
Miao, X., Lin, J., & Bian, F. (2020). Utilization of discarded crop straw to produce cellulose nanofibrils and their assemblies. *Journal of Bioresources and Bioproducts, 5*(1), 26–36. https://doi.org/10.1016/J.JOBAB.2020.03.003
Mohite, D. P., Mahadik-Khanolkar, S., Luo, H., Lu, H., Sotiriou-Leventis, C., & Leventis, N. (2013). Polydicyclopentadiene aerogels grafted with PMMA: I. Molecular and interparticle crosslinking. *Soft Matter, 9*, 1516–1530.
Pääkkö, M., Vapaavuori, J., Silvennoinen, R., Kosonen, H., Ankerfors, M., Lindström, T. Ikkala, O., … (2008). Long and entangled native cellulose I nanofibers allow flexible aerogels and hierarchically porous templates for functionalities. *Soft Matter, 4*(12), 2492–2499.
Pereira, A. L. S., Feitosa, J. P. A., Morais, J. P. S., & Rosa, M.d. F. (2020). Bacterial cellulose aerogels: Influence of oxidation and silanization on mechanical and absorption properties. *Carbohydrate Polymers, 250*, Article 116927. https://doi.org/10.1016/J.CARBPOL.2020.116927
Perumal, A. B., Nambiar, R. B., Moses, J. A., & Anandharamakrishnan, C. (2022). Nanocellulose: Recent trends and applications in the food industry. *Food Hydrocolloids, 127*, Article 107484. https://doi.org/10.1016/J.FOODHYD.2022.107484
Pircher, N., Carbajal, L., Schimper, C., Bacher, M., Rennhofer, H., Nedelec, J. M. Liebner, F., … (2016). Impact of selected solvent systems on the pore and solid structure of cellulose aerogels. *Cellulose, 23*(3), 1949–1966. https://doi.org/10.1007/S10570-016-0896-Z/TABLES/5
Reshmy, R., Philip, E., Madhavan, A., Pugazhendhi, A., Sindhu, R., Sirohi, R.Binod, P., … (2022). Nanocellulose as green material for remediation of hazardous heavy metal contaminants. *Journal of Hazardous Materials, 424*, Article 127516. https://doi.org/10.1016/J.JHAZMAT.2021.127516
Reshmy, R., Philip, E., Paul, S. A., Madhavan, A., Sindhu, R., Binod, P.Sirohi, R., … (2020). Nanocellulose-based products for sustainable applications-recent trends and possibilities. *Reviews in Environmental Science and Biotechnology, 19*(4), 779–806. https://doi.org/10.1007/S11157-020-09551-Z
Salimi, S., Sotudeh-Gharebagh, R., Zarghami, R., Chan, S. Y., & Yuen, K. H. (2019). Production of nanocellulose and its applications in drug delivery: A critical review. *ACS Sustainable Chemistry and Engineering, 7*(19), 15800–15827. https://doi.org/10.1021/ACSSUSCHEMENG.9B02744
Segal, L., Creely, J. J., Martin, A. E., & Conrad, C. M. (1959). An empirical method for estimating the degree of crystallinity of native cellulose using the X-ray diffractometer. *Textile Research Journal, 29*(10), 786–794.
Sehaqui, H., Zhou, Q., & Berglund, L. A. (2011). High-porosity aerogels of high specific surface area prepared from nanofibrillated cellulose (NFC). *Composites Science and Technology, 71*(13), 1593–1599.
Stenstad, P., Andresen, M., Tanem, B. S., & Stenius, P. (2008). Chemical surface modifications of microfibrillated cellulose. *Cellulose, 15*(1), 35–45.
Tan, C., Fung, B. M., Newman, J. K., & Vu, C. (2001). Organic aerogels with very high impact strength. *Advanced Materials, 13*(9), 644–646.
Trache, D., Tarchoun, A. F., Derradji, M., Hamidon, T. S., Masruchin, N., Brosse, N., & Hussin, M. H. (2020). Nanocellulose: From fundamentals to advanced applications. *Frontiers in Chemistry, 8*, 392. https://doi.org/10.3389/FCHEM.2020.00392/BIBTEX
Zhai, T., Zheng, Q., Cai, Z., Xia, H., & Gong, S. (2016). Synthesis of polyvinyl alcohol/cellulose nanofibril hybrid aerogel microspheres and their use as oil/solvent superabsorbents. *Carbohydrate Polymers, 148*, 300–308. https://doi.org/10.1016/J.CARBPOL.2016.04.065
Zhang, C., Zhai, T., & Turng, L.-S. (2017). Aerogel microspheres based on cellulose nanofibrils as potential cell culture scaffolds. *Cellulose, 24*(7), 2791–2799.
Zhang, W., Zhang, Y., Lu, C., & Deng, Y. (2012). Aerogels from crosslinked cellulose nano/micro-fibrils and their fast shape recovery property in water. *Journal of Materials Chemistry, 22*(23), 11642–11650.
Zou, Y., Zhao, J., Zhu, J., Guo, X., Chen, P., Duan, G.Li, Y., … (2021). A mussel-inspired polydopamine-filled cellulose aerogel for solar-enabled water remediation. *ACS Applied Materials and Interfaces, 13*(6), 7617–7624. https://doi.org/10.1021/ACSAMI.0C22584/SUPPL_FILE/AM0C22584_SI_001.PDF